Mo3+ hydride as the common origin of H2 evolution and selective NADH regeneration in molybdenum sulfide electrocatalysts

Mo^{3+} Hydride as the Common Origin of Efficient H_2 Evolution and Selective NADH Regeneration Activity in Molybdenum Sulfide Electrocatalysts

Jeremy A. Bau[1], Abdul-hamid Emwas[2], Pavlo Nikolaienko[1], Areej A. Aljarb[1,3], Vincent Tung[1], Magnus Rueping[1]

[1]KAUST Catalysis Center, Physical Sciences and Engineering Division, King Abdullah University of Science and Technology (KAUST), Thuwal, Saudi Arabia

[2]Imaging and Characterization Laboratory, KAUST, Thuwal, Saudi Arabia

[3]Department of Physics, King Abdulaziz University, Jeddah, Saudi Arabia

Abstract: Hydride transfers are key to a number of economically and environmentally important reactions, including H_2 evolution and NADH regeneration. Therefore, the electrochemical generation of reactive hydrides has the potential to drive the electrification of chemical reactions to improve their sustainability for a green economy. Catalysts containing molybdenum (Mo) have recently been recognized as amongst the most promising non-precious catalysts for H_2 evolution, but the mechanism of Mo in conferring this activity remains debated. In this work, we use a modified EPR setup to demonstrate the presence and catalytic role of a trapped Mo^{3+} hydride in amorphous Mo sulfide (*a*-MoS_x), one of the most active non-noble H_2 evolution catalysts yet reported. We further confirm that this hydride is active for the selective electrochemical hydrogenation of the biologically important energy carrier NAD to its active NADH form and therefore utilized for biocatalysis, and that this reactivity applies to other HER-active forms of Mo sulfide. Our results represent the first direct experimental evidence of an immediate role for Mo in heterogeneous H_2 evolution, placing a paramagnetic Mo center, as opposed to its partner atoms,

as an HER-active site with uniquely high activity for hydride formation and transfer. This mechanistic finding also reveals that Mo sulfides have potential as economic electrocatalysts for NADH regeneration in biocatalysis.

Introduction

The direct conversion of electricity to chemicals has profound implications for society, nowhere more acutely than with regards to energy. By 2040, the Organization of Petroleum Exporting Countries estimates that world oil demand for energy will reach 100.7 million barrels of oil per day[1], most of which must be replaced by carbon-neutral energy carriers and chemical intermediates to avoid catastrophic environmental consequences. "Green" H_2 generated from water electrolysis powered by renewable energy is a strong candidate as an alternative energy vector and carbon-neutral reducing agent, but its mass implementation requires the development of earth-abundant catalysts for the H_2-evolution reaction (HER) and the O_2-evolution reaction, both of which remain dominated by precious metals[2–4]. A successful zero-carbon transition would also require the replacement of traditional high temperature chemical processes with cleaner alternatives that function under facile conditions, such as via bio- or electrocatalysis[5,6]. In the case of electrocatalysis, expanding the scope of mechanistic understandings beyond electron transfers is vital for the development of more complicated reactions.

For the HER, Mo-based catalysts, namely NiMo[7–9] and Mo sulfides[10–15] (especially amorphous Mo sulfide (*a*-MoS_x))[14–18], are amongst the best-performing non-precious catalysts discovered so far[19], with potential for Pt-like activity[20,21]. Yet despite the prevalence of Mo in heterogeneous HER electrocatalysts, a direct role for Mo in the reaction (such as the formation of a metal hydride) has remained experimentally unresolved[15,22–24]. In Mo sulfides, a thiol-like

mechanism is instead favored due to the strong hydrogen binding energy of metallic Mo which should lead to poor HER activity (Fig. 1a)[20]. However, the existence of HER-active single-atom molecular Mo catalysts that are non-zero valent and sulfide-free[25,26] demonstrates that chemically reactive H_2 intermediates can be formed on Mo active sites. The involvement of a metal hydride intermediate in Mo-based catalysts would provide an explanation for the uniquely high activity for HER in these systems as well as assist in the design of future catalysts for the HER and electrochemical hydride transfers.

The transfer of energy through hydrides is of particular significance to the field of biocatalysis, where one quarter of all known enzymes, known as oxidoreductases, are capable of catalyzing electron and hydride transfers in the presence of hydride-bearing co-factors[27]. The vast majority of oxidoreductases (90%) rely on the biological energy carrier nicotinamide adenine dinucleotide (NAD) and its reduced, hydrogenated form (NADH) or their phosphorylated forms (NADP(H)) as co-factors[28]. Selective, economical NAD(P)H regeneration remains a significant barrier to the enzymatic preparation of complex organic molecules, as the prices of the reduced forms are prohibitively expensive ($3,000 and $215,000 USD/mol, respectively, in 2011)[29]. Electrochemical NAD(P)H regeneration has long been considered promising, but single electron transfers often result in the formation of biologically inactive NAD dimers or 1,2- and 1,6-dihydropyridine products[27]. The ideal electrochemical catalyst for NAD(P)H regeneration would therefore avoid single electron transfers and be capable of direct hydride transfer. Metals with strong hydride formation energies such as Ti have been shown to minimize single electron transfers[30]. Mo, like Ti, has a large metal hydride bond strength[31].

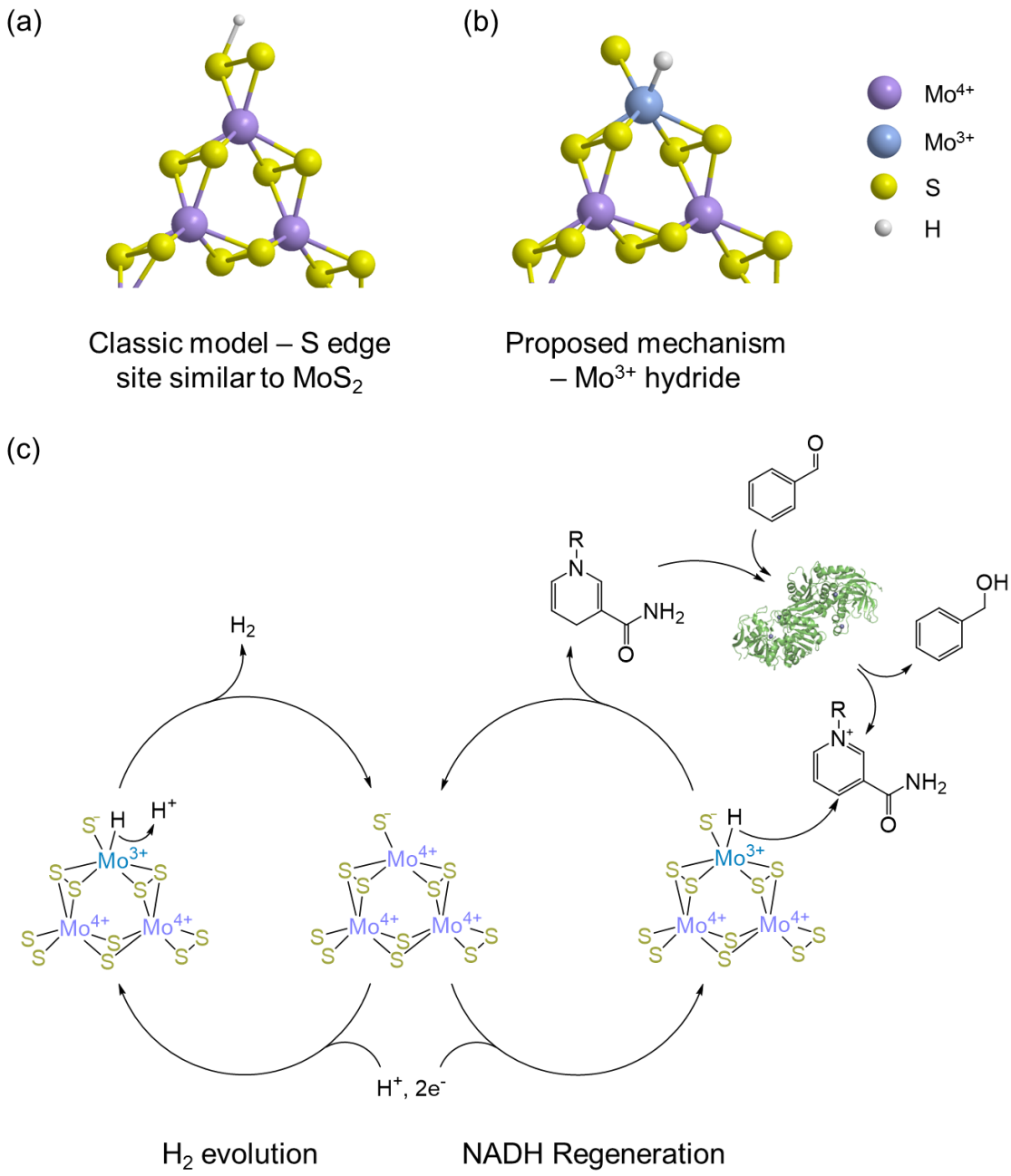

Fig. 1. Schemes of (a) the classic MoS_2 edge site-based HER mechanism in contrast to (b) the Mo^{3+} hydride mechanism discussed in this study. (c) Plausible reaction mechanism of how Mo^{3+} hydride in *a*-MoS_x catalyzes the HER and NADH regeneration mechanisms, and is subsequently regenerated.

In this study, we demonstrate the specific reduction of NAD and its analogue N-methyl nicotinamide (NMN), to their high-energy dihydropyridine derivatives using Mo sulfide catalysts, demonstrating the hydride nature of the Mo-H bond and its ability to catalyze transfer hydrogenation reactions using water as a hydride source. Our discovery was driven by the direct observation via electron paramagnetic resonance (EPR) spectroscopy of a trapped Mo^{3+} hydride in pre-catalytic *a*-MoS_x, confirming for the first time that Mo hydrides can form under HER conditions in heterogeneous Mo electrocatalysts (Fig. 1b). Roles for both Mo^{3+} and the hydride in the HER using Mo sulfides have never been conclusively identified due to the metastability of both states; their simultaneous existence has never even been proposed. Thus, the identification of a Mo^{3+} hydride species as an active site for electrochemical hydrogenation reactions in *a*-MoS_x thus serves as a "missing link" that unlocks important aspects in the understanding and design of Mo-based heterogeneous electrocatalysts for the HER and beyond.

Results

The Mo^{3+} hydride species was captured during the electrodeposition of *a*-MoS_x from MoS_4^{2-} solutions during cyclic voltammetry (CV), in which MoS_3 is deposited at anodic potentials and subsequently reduced to *a*-MoS_x at cathodic potentials close to the onset of the HER[14]. Inspired by the recent use of EPR in examining battery electrode processes[32,33], we modified an EPR setup to measure the oxidation states of paramagnetic species in complex electrocatalysts by combining a standard Wilmad-LabGlass electrolytic EPR flat cell with homemade flat wire electrodes. Catalyst is deposited on the flat wire so that it fits into the flat cell, resulting in minimal microwave interactions with both electrolyte and metal. Consequently, signal from catalyst deposited on the wire can be acquired (Extended Data Fig. 1). To prepare a sample suitable for EPR measurements,

a-MoS_x was deposited on the flat Au electrode and loaded into the EPR flat cell filled with tetrahydrofuran (THF). If the deposition was ended on the cathodic edge of the scan range, the resulting catalyst exhibited an isotropic EPR spectrum as shown in Fig. 2a. The spectrum itself was centered at 2.014, typical of the characteristic g-value[26] for Mo^{3+}, and had an average peak separation of 31 G, making it dissimilar to sulfide-related paramagnetic states in MoS_2[34,35] that have smaller peak separations (≤10 G) and g-values at 2.002. The EPR signal of the electrodes rapidly disappeared if the electrode was not immediately isolated under dry, O_2-free conditions, reflecting the metastability of Mo^{3+}.

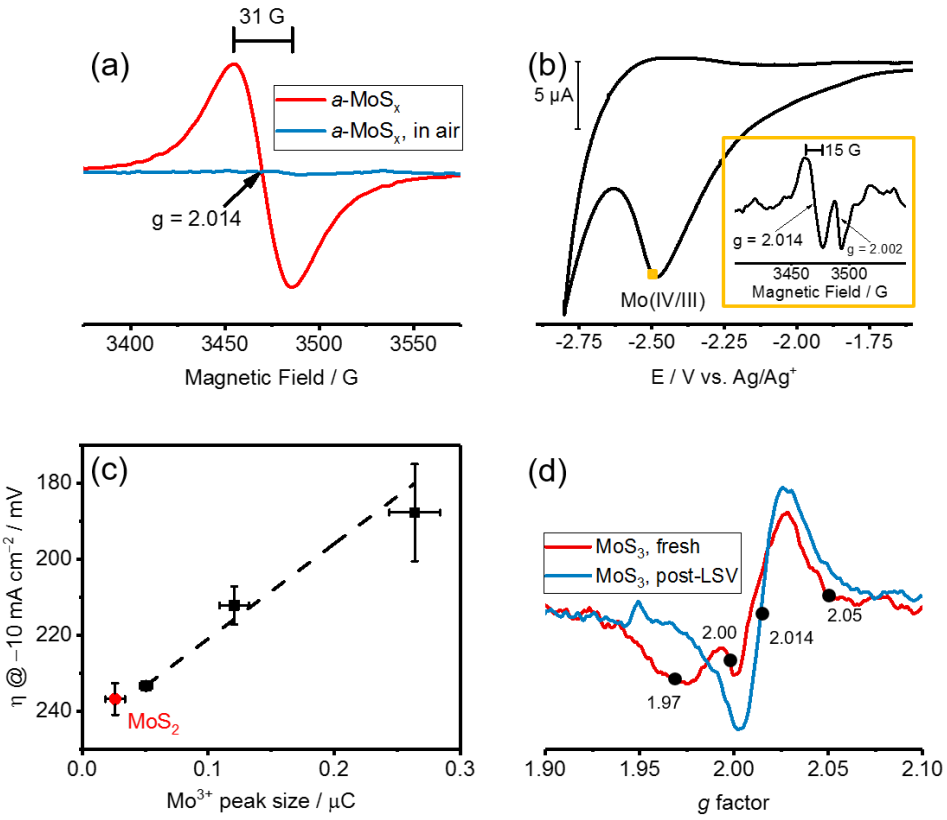

Fig. 2. EPR and electrochemical evidence for a Mo^{3+} hydride in *a*-MoS_x. (a) EPR spectra of a trapped Mo^{3+} hydride. (b) Cyclic voltammogram of *a*-MoS_x in 0.2 M Bu_4N PF_6/THF. *Inset*, EPR spectrum of *a*-MoS_x reduced at –2.5 V vs. Ag/Ag^+. Signal at 2.002 arises from the reduction of the

electrolyte. (c) Correlation plot of Mo^{3+} peak size in 0.2 M Bu_4N PF_6/THF vs. HER activity as measured by η at −10 mA cm^{-2} in 0.05 M H_2SO_4. (d) EPR spectra of anodically deposited *a*-MoS_x after deposition and after conditioning by voltammetric sweep to the HER potential.

Although the Mo^{3+} EPR signal could be lost upon oxidation, it could also be partly restored if *a*-MoS_x was reduced in organic electrolyte (0.2 M Bu_4N PF_6/THF, Fig. 2b) within the cavity of the EPR spectrometer, revealing the re-emergence of the Mo^{3+} signal with a width of 15 G (inset). The contrast in peak-to-peak width between the original signal and the reduced form in aprotic electrolyte indicates the presence of hyperfine coupling between a spin-active nuclei and the Mo^{3+} center. As less than 1% of naturally occurring S has a nuclear spin[36], the only other possible candidate atom was H, revealing the presence of a hydride directly bound to Mo^{3+}. Further confirmation of the bound hydride was modeled using EasySpin[37], where a hydride hyperfine coupling constant of ~34.5 was fit to the peak, within range of previously reported Mo^{3+} hydrides (Extended Data Figure 2, Table 1). These EPR spectra therefore represent the first direct evidence for the formation of a hydride associated with Mo^{3+} in *a*-MoS_x. Only one major reduction peak was observed during a cathodic sweep from open circuit potential, demonstrating that the resting state of the catalyst was Mo^{4+}, in line with X-ray photoelectron studies[14–16]. Coulometric measurements of the reduction event revealed that it corresponded to 40% of the Mo present in the *a*-MoS_x catalyst as determined by inductively coupled plasma – optical emission spectroscopy (ICP-OES), suggesting that 40% of Mo in *a*-MoS_x can be converted to the Mo^{3+} state. In comparison, the Mo hydride species in freshly deposited *a*-MoS_x represented 2% of the total Mo as determined by spin counting. Furthermore, by using *a*-MoS_x electrodes with increasing deposition amounts, the area of the peak as determined using coulometry was found to form a linear correlation with the activity of the *a*-MoS_x itself as measured by overpotential at −10 mA

cm^{-2} in 0.05 M H_2SO_4 (Fig. 2c). This relationship between Mo^{3+} peak size and HER activity was also found to be relevant to MoS_2, as HER-active MoS_2 prepared by autoclave synthesis (for MoS_2) was found to fit the trend (Extended Data Fig. 4)[38]. Alternately, epitaxially grown, single-crystal (less defective) MoS_2 had no Mo^{3+} peak nor significant HER activity (Extended Data Fig. 8)[39]. Therefore, the amount of reducible Mo^{3+} correlates directly to the HER activity of a given Mo sulfide electrode and can be used as a quantifiable benchmark for the HER activity of Mo sulfides.

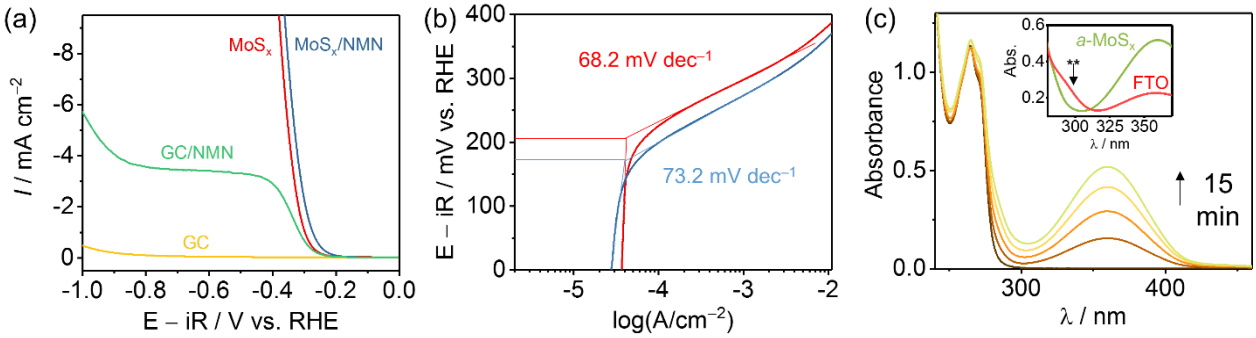

Fig. 3. Electrochemical and absorption characteristics of NMN reduction by *a*-MoS_x. (a) Voltammograms of *a*-MoS_x and GC in 0.5 M K_2CO_3 with and without NMN. (b) Linear sweep voltammograms of *a*-MoS_x for the HER and NMN reduction. (c) UV-vis spectra of 5 mM NMN solution being reduced over time in 0.5 M K_2CO_3 solution (pH 10) by *a*-MoS_x electrode (−10 mA cm^{-2}). Inset, reduction of NMN by FTO. Dimer decomposition peak marked **.

The existence of an isotropic Mo^{3+} hydride in *a*-MoS_x provides valuable insights into the structure of the catalyst. For example, Mo^{5+} in anodically deposited Mo_3S_{13} is coordinated by a number of theoretically equivalent S atoms, but does not have an isotropic EPR signal (Fig. 2d), reflecting the inequivalent positioning of S atoms around the Mo center[40]. In contrast, the isotropic Mo^{3+} spectrum correlates with the equivalent coordination of atoms (H and S) around the Mo center. Since *a*-MoS_x (at least initially) resembles Mo_3S_{13} clusters[22], the only possibility that could explain the isotropic hydride signal is the presence of a hydride within a Mo_3S_{11}(H) cluster. The

loss of two S atoms – the apical S as well as one of the disulfide S – results in Mo being equivalently coordinated by six atoms (five S and one H) while accounting for the presence of a metal hydride. The transformation between Mo_3S_{13} and $Mo_3S_{11}(H)$ is labile, as the Mo^{5+} EPR signal in anodically-deposited MoS_3 could be rapidly converted to the Mo^{3+} hydride signal upon a single linear potential sweep to the HER potential in aqueous electrolyte.

The role for a hydride intermediate during the HER on *a*-MoS_x is not just of fundamental interest; Mo hydrides have also been demonstrated as amongst effective non-noble metal hydrogenation catalysts[41], suggesting that *a*-MoS_x could be used in electrocatalytic transfer hydrogenation reactions using water as a hydride source, particularly for the biocatalytically-significant recycling of NADH. We therefore sought catalytic evidence for a metal hydride by studying the reduction of N-methyl nicotinamide (NMN), an analogue of NAD, which is also hydrogenated to a 1,4-dihydropyridine[42]. However, NMN is more ideal for distinguishing reduction mechanisms as its single-electron transfer products have distinct spectroscopic (NMR and UV-vis) properties[42–44], unlike NAD[45]. Electrochemical reduction of NMN in electrolyte (0.5 M K_2CO_3, pH 10, 5 mM NMN) by *a*-MoS_x results in a 30 mV positive shift of the onset of catalysis compared to the HER (Fig. 3a,b), which is reasonable given that NAD^+ reduction to NADH has a less cathodic electrode potential compared to the HER[46]. NMN reduction otherwise does not affect the activity of the HER, as evidenced by the similarity in linear sweep voltammograms between *a*-MoS_x in NMN-containing and NMN-free electrolytes. In contrast, common electrode materials such as glassy carbon (GC) reduce NMN in two sequential reduction processes corresponding to the two different reduction mechanisms discussed above. Furthermore, the onset of the one-electron reduction happens close to the HER onset for *a*-MoS_x. Therefore, the mechanism of NMN

reduction (1,4-dihydropyridine or dimer followed by breakdown) can be used to determine the role and presence of a metal hydride.

To distinguish the two reduction mechanisms for the reaction on *a*-MoS_x, UV-visible spectroscopy was used to analyze the NMN electrolyte before and after electrolysis using *a*-MoS_x. The 1,4-dihydropyridine absorbs strongly at 360 nm while the dimer and its decomposition products have absorption peaks centered at both 360 and 298 nm[43]. The NMN electrolyte gradually formed a peak at 360 nm when electrolyzed with *a*-MoS_x at a current density of –10 mA cm^{-2} (η = ~–450 mV) with no prominent features at 298 nm being observed (Fig. 3c). In comparison, a fluorine-doped tin oxide (FTO) electrode electrolyzed at the same potential produced both a less intense 360 nm peak as well as the 298 nm dimer decomposition product peak (inset). The 360 nm peak was also less intense with electrolyte from FTO as compared to *a*-MoS_x.

As a final confirmation that *a*-MoS_x directly reduces NMN to the 1,4-dihydropyridine derivative without proceeding through single-electron transfer, the electrochemical reduction was additionally carried out in both the normal electrolyte as well as deuterated solution (D_2O/K_2CO_3/adjusted to pH 10 using D_2SO_4) followed by nuclear magnetic resonance (NMR) spectroscopy of the isolated product. Deuteration at C4 of NMN should lead to the formation of a CDH motif (Fig. 4a), resulting in the appearance of a triplet peak at the given NMR shift. Indeed, a triplet peak formed at 22.36 ppm in the ^{13}C NMR spectra that was replaced by a singlet peak in the otherwise identical spectra of the product of the H_2O reaction (Fig. 4b,c)[44]. A less intense triplet was also observed at 49.93 ppm, suggesting that the CDH motif was formed at the C6 position as well based on its similar position in 1,6-NADH[47]. Deuterated species were found in the ^2H-NMR spectrum of the isolated product; however, the 3.11 ppm peak corresponding to a deuterated C4 in the dihydropyridine structure was the most intense, confirming that the major hydrogenation

product was the 1,4-dihydropyridine (Fig. 4d). The deuterated species were also observed in peak broadening between the ^{1}H-NMR spectra of the deuterated and non-deuterated products (Fig. 4e,f). The direct formation of deuterated product without the dimerization side-reaction is confirmation that the Mo hydride is chemically reactive. These results demonstrate that Mo hydride, and specifically Mo^{3+} hydride, is the intermediate to H_2 evolution and nicotinamide reduction in Mo sulfides (Fig. 1c). Upon The evolution of H_2 evolution, Mo^{3+} is oxidized to Mo^{4+} and ultimately reduced to Mo^{3+} upon reformation of the hydride.

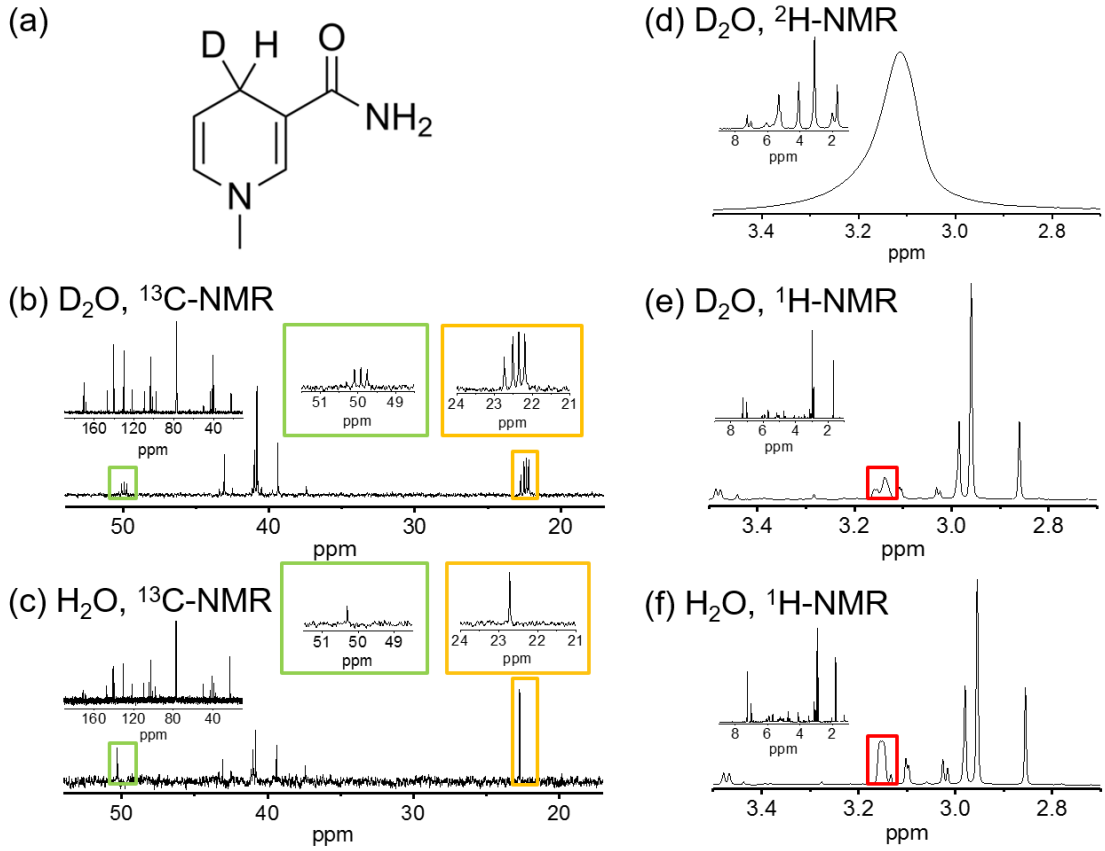

Fig. 4. Reduction of NMN to 1,4-dihydropyridine derivative. (a) Expected structure of a mixed HD 1,4-dihydropyridine. (b,c) ^{13}C-NMR spectra of the isolated products when the reaction is carried out in D_2O and H_2O, respectively. Highlighted insets in (b) are the triplet peaks. (d) ^{2}H-

NMR spectrum of the products of the D_2O reaction. (e,f) ^{1}H-NMR spectra of the products in the D_2O and H_2O reactions, respectively. A full spectrum is included in each inset.

Based on the ability of *a*-MoS_x to specifically hydrogenate NMN to its dihydropyridine derivative, the potential of *a*-MoS_x for NADH regeneration was tested for the enzymatic hydrogenation of benzaldehyde to benzyl alcohol using alcohol dehydrogenase (ADH) from *Saccharomyces cerevisiae* (Fig. 5a). Selective regeneration of NADH without formation of the inactive $(NAD)_2$ dimer or inactive 1,2- and 1,6-dihydropyridine isoforms remains an important challenge in the application of electrocatalysis to biocatalysis, often necessitating the use of homogeneous, often noble metal-based mediators[27]. The purity of NADH regenerated by *a*-MoS_x was examined using an ultrahigh performance liquid chromatography system coupled to an orbitrap tribrid mass spectrometer (UHPLC-MS) in pH 9 electrolyte. After regeneration for 30 to 60 minutes at constant potential (−600 mV vs. RHE, average current ~7 mA), the quantities of produced dimer were consistently marginal or undetectable (<0.1%, Fig. 5b, see Extended Data for additional information), consistently reflecting the results of electrochemical NMN reduction where no dimer products were observed to form. As NADH isomers can also be formed as a result of electron transfer followed by protonation, NMR was used to confirm that no 1,2- or 1,6-NADH isomers were present (Extended Data Fig. 21), especially as partial 1,6-dihydropyridine formation had been observed with NMN (Fig. 4).

Since direct NADH regeneration proved promising, the utility of *a*-MoS_x for direct biocatalysis was tested using the synthesis of benzyl alcohol from benzaldehyde in the presence of enzyme and tenfold excess of benzaldehyde (10 mM) to NAD (1 mM). After 3 hours, 78% conversion was achieved, rising to 87% over 4 hours (Fig. 5c). Therefore, over eight complete turnovers of NAD/NADH by *a*-MoS_x were carried out over the course of the reaction.

Simultaneously, NAD conversion to NADH increased as the reaction proceeded, reaching quantitative reduction at 3 hours as determined by two enzymatic NADH quantitation assays (Promega, Sigma-Aldrich), even as the rate of benzaldehyde conversion slowed. Naturally, NADH is rapidly consumed during the early stages of the reaction, but the enzymatic conversion of benzaldehyde appears to be the limiting step at later stages. As foam formation was observed as the reaction progressed, we hypothesize that co-generated H_2 was responsible for denaturing the enzyme over long time courses. As such the Faradaic efficiency for NADH formation fell as the reaction proceeded (Extended Data Fig. 22). *a*-MoS_x also had no activity for benzaldehyde hydrogenation in the absence of enzyme or NAD, underlining its selectivity for the nicotinamide system. This specificity is important as it would allow for *a*-MoS_x to be used in any future biocatalytic system without concerns that the catalyst could reduce other functional groups that might be present, obviating the need for protecting groups. We also note that the high yield of recycled 1,4-NADH as determined by enzymatic assay (in addition to confirmation of its purity by NMR and commercial NADH assays) clearly demonstrates that the formation of the 1,6 product from NMN (Figure 4) was avoided by the presence of a larger N1 substituent in NAD^+, resulting in greater steric hindrance at the C6 position than in NMN. The ability of *a*-MoS_x to carry out site-specific hydrogenation depending on the steric hindrance provided by the substrate provides a significant contrast to Pt-based systems, where pyridine ring adsorption to the Pt surface results in multiple site selectivity[48].

To confirm that the HER and NAD reduction arise from a common origin and mechanism, we tested the ability of other Mo sulfides to carry out NAD reduction in addition to previous experiments for the HER. Hydrothermally-prepared MoS_2 demonstrated similar activity (76% after 3 hours), but the epitaxially grown and continuously single-crystal (less defective) MoS_2 was

inactive (Fig. 5d). Since, like *a*-MoS_x, hydrothermal MoS_2 is similarly rich in Mo^{3+}-generating sites, and defect-free MoS_2 is low in such sites, we can therefore conclude that defective sites in Mo sulfides where Mo^{3+}-H is generated are the common active sites for both the HER and NAD reduction. Such selective NAD reduction underlines the consistent and specific nature by which Mo sulfide electrocatalysts under HER potentials engage in hydride (as opposed to electron) transfer despite being held at more negative potentials than the NAD dimerization potential[49]. For comparison, GC and Ti catalysts that have been previously reported for specific and direct NADH regeneration were compared to the tested Mo sulfides[30,50]. However, both were poorly effective under identical conditions, resulting in 4% (GC) and 7% (Ti) conversion of benzaldehyde to benzyl alcohol, respectively, over the course of 3 hours. Furthermore, neither catalyst reached quantitative NADH regeneration under the tested conditions, in contrast to the defective Mo sulfides.

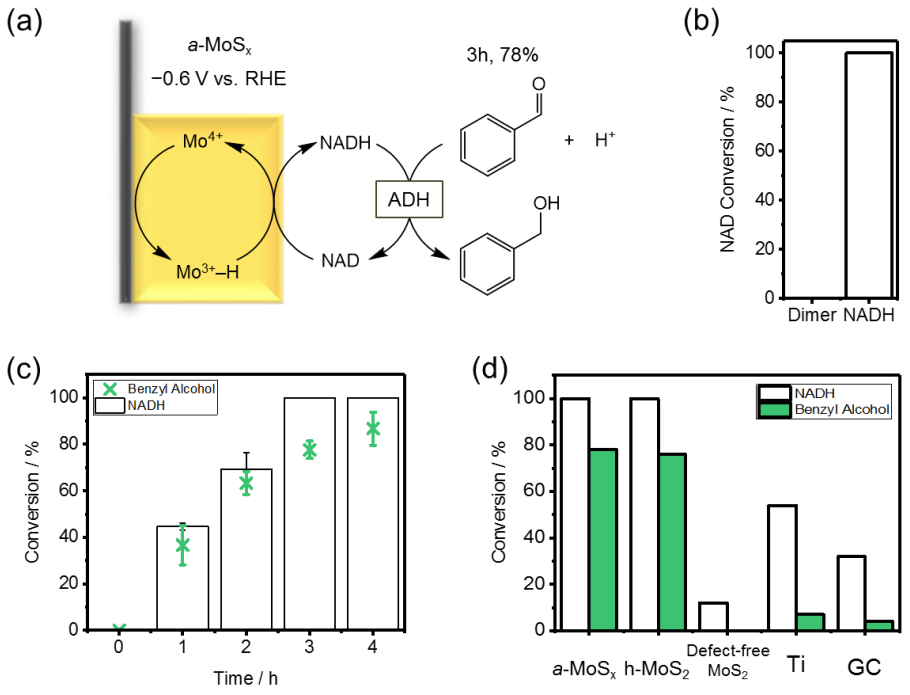

Fig. 5. (a) Conversion of benzaldehyde to benzyl alcohol by *S. cerevisiae* ADH using *a*-MoS_x as a catalyst for NAD reduction to NADH. Reaction conditions: 2 µmol NAD, 20 µmol benzaldehyde,

5.6 mg ADH, in 2 mL 0.1 M *N*-cyclohexyl-2-aminoethanesulfonic acid (CHES)/0.1 M K_2SO_4 (pH 9) electrolyte. In all cases, the Pt counter electrode was separated from the main compartment by a Nafion membrane with 0.05 M H_2SO_4. (b) Ratio of NAD dimer to NADH formed during electrolysis by holding at −600 mV as assayed by UHPLC-MS. To facilitate UHPLC, 0.1 M ammonium acetate (pH 9) was used as the electrolyte. (c) Time course of NADH regeneration and biocatalytic benzyl alcohol synthesis using *a*-MoS_x in 0.1 M CHES/0.1 M K_2SO_4 (pH 9). (d) NADH regeneration and biocatalytic benzyl alcohol synthesis after 3 hours using *a*-MoS_x, hydrothermal MoS_2 (h-MoS_2), defect-free MoS_2, Ti, and GC. NADH regeneration was carried out as in (b), in the absence of enzyme and benzaldehyde.

Finally, we discuss the implications of Mo^{3+} hydride formation for both the HER and NAD regeneration. Traditionally, the primary thiol-based model[20] considered that Mo sulfides evolve H_2 through the recombination of two active hydrogen species (H*, hydrogen with a single electron) on S atoms from thiol-like precursors. However, by demonstrating non-dimerization and high 1,4-dihydropyridine yield for both NAD and NMN, it is clear that a hydride must be the intermediate catalytic species. Furthermore, the loss of H* from a thiol would yield a thiyl radical that should have in turn reacted with the reduced NMN to yield decomposition products, as is the case for NADH[51]. We further demonstrate the viability of a hydride mechanism by testing the HER activity of ultrathin (5 cycle, to minimize the possible contribution of bulk Mo sulfide) *a*-MoS_x poisoned by maleimide to inhibit thiol formation[52]. Although x-ray photoelectron spectra (XPS) of the poisoned surfaces suggested that one quarter of all S were poisoned (Extended Data Fig. 23, Table 2), poisoning had no significant effect on HER activity in either proton-rich or proton-poor electrolytes, excluding significant catalytic contributions from thiols regardless of proton concentration (Extended Data Fig. 24). It is possible that previous observations of thiols forming

during the HER[53,54] originate from proton accumulation at the cathode as a result of applied potentials. Electronic effects from sulfur also cannot be excluded[34,55]. Nonetheless, the selective reduction of nicotinamide systems strongly suggests that the Mo^{3+} hydride trapped and observed in EPR is the primary reactive intermediate, thereby allowing Mo sulfides to avoid unwanted dihydropyridine and dimer formation during nicotinamide reduction.

Conclusion

In conclusion, we have demonstrated that hydride-forming Mo sulfides are economical and selective electrocatalysts for NADH regeneration, in addition to being effective HER catalysts, as a result of the formation of Mo^{3+} hydride active species at cathodic potentials in aqueous solutions. The central role of the hydride species in carrying out both reactions as well as the specificity endowed in nicotinamide reduction provides a convincing picture of the mechanism of reactivity of these hydrides for both reactions. Considering the prevalence of Mo amongst effective non-noble HER catalysts, this study justifies the further design and exploration of Mo-based HER catalysts. Finally, the ability of Mo sulfide electrocatalysts to form and transfer hydrides in exclusion of single electron transfers not only opens a cost-effective route for application in biocatalysis, but points to a new strategy and paradigm for electrocatalyst design.

References and Notes:

1. Organization of Petroleum Exporting Countries. World Oil Outlook 2040. (2017).
2. Roger, I., Shipman, M. A. & Symes, M. D. Earth-abundant catalysts for electrochemical and photoelectrochemical water splitting. *Nature Reviews Chemistry* **1**, 0003 (2017).
3. Montoya, J. H. *et al.* Materials for solar fuels and chemicals. *Nat. Mater.* **16**, 70–81 (2017).

4. Seh, Z. W. *et al.* Combining theory and experiment in electrocatalysis: Insights into materials design. *Science* **355**, eaad4998 (2017).
5. Sheldon, R. A. & Woodley, J. M. Role of Biocatalysis in Sustainable Chemistry. *Chem. Rev.* **118**, 801–838 (2018).
6. Kibria, M. G. *et al.* Electrochemical CO2 Reduction into Chemical Feedstocks: From Mechanistic Electrocatalysis Models to System Design. *Advanced Materials* **31**, 1807166 (2019).
7. Zhang, J. *et al.* Efficient hydrogen production on $MoNi_4$ electrocatalysts with fast water dissociation kinetics. *Nature Communications* **8**, 15437 (2017).
8. Csernica, P. M. *et al.* Electrochemical Hydrogen Evolution at Ordered Mo_7Ni_7. *ACS Catal.* **7**, 3375–3383 (2017).
9. Bau, J. A. *et al.* On the reconstruction of NiMo electrocatalysts by operando spectroscopy. *J. Mater. Chem. A* **7**, 15031–15035 (2019).
10. Jaramillo, T. F. *et al.* Identification of Active Edge Sites for Electrochemical H_2 Evolution from MoS_2 Nanocatalysts. *Science* **317**, 100–102 (2007).
11. Li, H. *et al.* Activating and optimizing MoS_2 basal planes for hydrogen evolution through the formation of strained sulphur vacancies. *Nat. Mater.* **15**, 48–53 (2016).
12. Ding, Q., Song, B., Xu, P. & Jin, S. Efficient Electrocatalytic and Photoelectrochemical Hydrogen Generation Using MoS_2 and Related Compounds. *Chem* **1**, 699–726 (2016).
13. Chia, X. & Pumera, M. Characteristics and performance of two-dimensional materials for electrocatalysis. *Nature Catalysis* **1**, 909 (2018).
14. Merki, D., Fierro, S., Vrubel, H. & Hu, X. Amorphous molybdenum sulfide films as catalysts for electrochemical hydrogen production in water. *Chem. Sci.* **2**, 1262–1267 (2011).
15. Tran, P. D. *et al.* Coordination polymer structure and revisited hydrogen evolution catalytic mechanism for amorphous molybdenum sulfide. *Nat. Mater.* **15**, 640–646 (2016).
16. Benck, J. D., Chen, Z., Kuritzky, L. Y., Forman, A. J. & Jaramillo, T. F. Amorphous Molybdenum Sulfide Catalysts for Electrochemical Hydrogen Production: Insights into the Origin of their Catalytic Activity. *ACS Catal.* **2**, 1916–1923 (2012).

17. Escalera-López, D., Lou, Z. & Rees, N. V. Benchmarking the Activity, Stability, and Inherent Electrochemistry of Amorphous Molybdenum Sulfide for Hydrogen Production. *Advanced Energy Materials* **9**, 1802614 (2019).
18. Morales-Guio, C. G. & Hu, X. Amorphous Molybdenum Sulfides as Hydrogen Evolution Catalysts. *Acc. Chem. Res.* **47**, 2671–2681 (2014).
19. Zhuang, Z., Huang, J., Li, Y., Zhou, L. & Mai, L. The Holy Grail in Platinum-Free Electrocatalytic Hydrogen Evolution: Molybdenum-Based Catalysts and Recent Advances. *ChemElectroChem* **6**, 3570–3589 (2019).
20. Hinnemann, B. *et al.* Biomimetic Hydrogen Evolution: MoS_2 Nanoparticles as Catalyst for Hydrogen Evolution. *J. Am. Chem. Soc.* **127**, 5308–5309 (2005).
21. Cao, Y. Roadmap and Direction toward High-Performance MoS2 Hydrogen Evolution Catalysts. *ACS Nano* **15**, 11014–11039 (2021).
22. Lassalle-Kaiser, B. *et al.* Evidence from in Situ X-ray Absorption Spectroscopy for the Involvement of Terminal Disulfide in the Reduction of Protons by an Amorphous Molybdenum Sulfide Electrocatalyst. *J. Am. Chem. Soc.* **137**, 314–321 (2015).
23. Xi, F. *et al.* Structural Transformation Identification of Sputtered Amorphous MoS_x as an Efficient Hydrogen-Evolving Catalyst during Electrochemical Activation. *ACS Catal.* **9**, 2368–2380 (2019).
24. Huang, Y., Nielsen, R. J., Goddard, W. A. & Soriaga, M. P. The Reaction Mechanism with Free Energy Barriers for Electrochemical Dihydrogen Evolution on MoS_2. *J. Am. Chem. Soc.* **137**, 6692–6698 (2015).
25. Karunadasa, H. I., Chang, C. J. & Long, J. R. A molecular molybdenum-oxo catalyst for generating hydrogen from water. *Nature* **464**, 1329–1333 (2010).
26. Prior, C. *et al.* EPR detection and characterisation of a paramagnetic Mo(III) dihydride intermediate involved in electrocatalytic hydrogen evolution. *Dalton Trans.* **45**, 2399–2403 (2016).
27. Wang, X. *et al.* Cofactor NAD(P)H Regeneration Inspired by Heterogeneous Pathways. *Chem* **2**, 621–654 (2017).
28. Wu, H. *et al.* Methods for the regeneration of nicotinamide coenzymes. *Green Chem.* **15**, 1773–1789 (2013).
29. Faber, K. Biocatalytic Applications. in *Biotransformations in Organic Chemistry: A Textbook* (ed. Faber, K.) 31–313 (Springer, 2011). doi:10.1007/978-3-642-17393-6_2.

30. Ali, I., Khan, T. & Omanovic, S. Direct electrochemical regeneration of the cofactor NADH on bare Ti, Ni, Co and Cd electrodes: The influence of electrode potential and electrode material. *Journal of Molecular Catalysis A: Chemical* **387**, 86–91 (2014).
31. Trasatti, S. Work function, electronegativity, and electrochemical behaviour of metals: III. Electrolytic hydrogen evolution in acid solutions. *Journal of Electroanalytical Chemistry and Interfacial Electrochemistry* **39**, 163–184 (1972).
32. González, J. R., Alcántara, R., Tirado, J. L., Fielding, A. J. & Dryfe, R. A. W. Electrochemical Interaction of Few-Layer Molybdenum Disulfide Composites vs Sodium: New Insights on the Reaction Mechanism. *Chem. Mater.* **29**, 5886–5895 (2017).
33. Sathiya, M. *et al.* Electron paramagnetic resonance imaging for real-time monitoring of Li-ion batteries. *Nature Communications* **6**, 6276 (2015).
34. Yin, Y. *et al.* Contributions of Phase, Sulfur Vacancies, and Edges to the Hydrogen Evolution Reaction Catalytic Activity of Porous Molybdenum Disulfide Nanosheets. *J. Am. Chem. Soc.* **138**, 7965–7972 (2016).
35. Cai, L. *et al.* Vacancy-Induced Ferromagnetism of MoS_2 Nanosheets. *J. Am. Chem. Soc.* **137**, 2622–2627 (2015).
36. Meija, J. *et al.* Isotopic compositions of the elements 2013 (IUPAC Technical Report). *Pure and Applied Chemistry* **88**, 293–306 (2016).
37. Stoll, S. & Schweiger, A. EasySpin, a comprehensive software package for spectral simulation and analysis in EPR. *Journal of Magnetic Resonance* **178**, 42–55 (2006).
38. Lu, Z. *et al.* Ultrahigh Hydrogen Evolution Performance of Under-Water "Superaerophobic" MoS_2 Nanostructured Electrodes. *Advanced Materials* **26**, 2683–2687 (2014).
39. Aljarb, A. *et al.* Ledge-directed epitaxy of continuously self-aligned single-crystalline nanoribbons of transition metal dichalcogenides. *Nat. Mater.* 1–7 (2020) doi:10.1038/s41563-020-0795-4.
40. Busetto, L., Vaccari, A. & Martini, G. Electron spin resonance of paramagnetic species as a tool for studying the thermal decomposition of molybdenum trisulfide. *J. Phys. Chem.* **85**, 1927–1930 (1981).
41. Bullock, R. M. Molybdenum and Tungsten Catalysts for Hydrogenation, Hydrosilylation and Hydrolysis. in *Catalysis without Precious Metals* 51–81 (John Wiley & Sons, Ltd, 2010). doi:10.1002/9783527631582.ch3.

42. Micheletti Moracci, F. *et al.* Electrochemical reduction of 1-benzyl-3-carbamoylpyridinium chloride, a nicotinamide adenine dinucleotide model compound. *J. Org. Chem.* **43**, 3420–3422 (1978).
43. Schmakel, C. O., Santhanam, K. S. V. & Elving, P. J. Nicotinamide and N'-Methylnicotinamide: Electrochemical Redox Pattern: Behavior of Free Radical, Dimeric, and Dihydropyridine Species. *J. Electrochem. Soc.* **121**, 345 (1974).
44. Erb, C. *et al.* Formation of N-methylnicotinamide in the brain from a dihydropyridine-type prodrug: Effect on brain choline. *Biochemical Pharmacology* **57**, 681–684 (1999).
45. Burnett, J. W. H., Howe, R. F. & Wang, X. Cofactor NAD(P)H Regeneration: How Selective Are the Reactions? *Trends in Chemistry* **2**, 488–492 (2020).
46. Wilson, D. F., Erecińska, M. & Dutton, P. L. Thermodynamic Relationships in Mitochondrial Oxidative Phosphorylation. *Annual Review of Biophysics and Bioengineering* **3**, 203–230 (1974).
47. Godtfredsen, S. E., Ottesen, M. & Andersen, N. R. On the mode of formation of 1,6-dihydro-NAD in NADH preparations. *Carlsberg Res. Commun.* **44**, 65 (1979).
48. H. Burnett, J. W. *et al.* Directing the H_2-driven selective regeneration of NADH via Sn-doped Pt/SiO_2. *Green Chemistry* (2022) doi:10.1039/D1GC04414A.
49. Steckhan, E. Electroenzymatic synthesis. in *Electrochemistry V* (ed. Steckhan, E.) 83–111 (Springer, 1994). doi:10.1007/3-540-57729-7_3.
50. Ali, I., Soomro, B. & Omanovic, S. Electrochemical regeneration of NADH on a glassy carbon electrode surface: The influence of electrolysis potential. *Electrochemistry Communications* **13**, 562–565 (2011).
51. Forni, L. G. & Willson, R. L. Thiyl and phenoxyl free radicals and NADH Direct observation of one-electron oxidation. *Biochem J* **240**, 897–903 (1986).
52. Vera-Hidalgo, M., Giovanelli, E., Navío, C. & Pérez, E. M. Mild Covalent Functionalization of Transition Metal Dichalcogenides with Maleimides: A "Click" Reaction for 2H-MoS_2 and WS_2. *J. Am. Chem. Soc.* **141**, 3767–3771 (2019).
53. Deng, Y. *et al.* Operando Raman Spectroscopy of Amorphous Molybdenum Sulfide (MoSx) during the Electrochemical Hydrogen Evolution Reaction: Identification of Sulfur Atoms as Catalytically Active Sites for H+ Reduction. *ACS Catal.* **6**, 7790–7798 (2016).

54. Chen, J. *et al.* Ag@MoS2 Core–Shell Heterostructure as SERS Platform to Reveal the Hydrogen Evolution Active Sites of Single-Layer MoS2. *J. Am. Chem. Soc.* **142**, 7161–7167 (2020).
55. Ting, L. R. L. *et al.* Catalytic Activities of Sulfur Atoms in Amorphous Molybdenum Sulfide for the Electrochemical Hydrogen Evolution Reaction. *ACS Catal.* **6**, 861–867 (2016).

Competing interests: None.

Additional information:

Extended data figures are available for this paper.

Reprints and permissions information is available at www.nature.com/reprints.

Original data are available from the corresponding authors upon reasonable request.